Acta Geotechnica (2016) 11:1249–1261
DOI 10.1007/s11440-016-0440-1

RESEARCH PAPER

Enhancement of a hypoplastic model for granular soil–structure interface behaviour

H. Stutz[1] · **D. Mašín**[2] · **F. Wuttke**[1]

Received: 30 July 2015 / Accepted: 20 January 2016 / Published online: 16 February 2016

Abstract Modelling of interfaces in geotechnical engineering is an important issue. Interfaces between structural elements (e.g., anchors, piles, tunnel linings) and soils are widely used in geotechnical engineering. The objective of this article is to propose an enhanced hypoplastic interface model that incorporates the in-plane stresses at the interface. To this aim, we develop a general approach to convert the existing hypoplastic model with a predefined limit state surface for sands into an interface model. This is achieved by adopting reduced stress and stretching vectors and redefining tensorial operations which can be used in the existing continuum model with few modifications. The enhanced interface model and the previous model are compared under constant-load, stiffness and volume conditions. The comparison is followed by a verification of two the approaches for modelling the different surface roughness. Subsequently, a validation between available experimental data from the literature versus simulations is presented. The new enhanced model gives improved predictions by the incorporation of in-plane stresses into the model formulation.

Keywords Hypoplasticity · Roughness · Sand–structure interface · Shear behaviour

✉ H. Stutz
hs@gpi.uni-kiel.de

D. Mašín
Masin@natur.cuni.cz

F. Wuttke
fw@gpi.uni-kiel.de

[1] Marine and Land Geotechnics/Geomechanics, Institute for Geoscience, Christian Albrechts Universität, Ludewig–Meyn–Str. 10, 24321 Kiel, Germany

[2] Faculty of Science, Charles University in Prague, Albertov 6, 12843 Prague 2, Czech Republic

1 Introduction

The contact between structural elements and granular soils is an important concern but are often neglected in finite element analysis in geotechnical engineering. Examples of the importance of advanced modelling of the interface zone between the soil and the structure are given for example by Costa D'Aguiar et al. [9], Day and Potts [10] and Mascarucci et al. [35].

Quantification of the importance of the soil–structure interface was pioneered by Potyondy [40] and Brumund and Leonards [7] through an intensive laboratory study. These early studies highlighted the importance of the particle mineralogy, moisture content of the soil, particle mean grain size and normal load on interface strength. Potyondy [40] tested granular, fine-grained and mixtures of both soils with respect to different structural materials in a modified direct shear test apparatus; he demonstrated that the type of soil as well as the structural material is of significant importance to the interface shear behaviour.

The fundamental research conducted by Potyondy [40] was followed by research concerning the different phenomena observed at the soil–structure interface, e.g., Refs. [11, 13, 15, 16, 39, 43, 44, 45, 48]. Fioravante et al. [16] summarised the following important points that influence soil–structure interface behaviour:

- Roughness of the surface
- Grain size
- Soil crushability
- Relative density of soil
- Constant normal stiffness K

The constant normal stiffness condition has been highlighted by different researchers [6, 12, 18, 38, 39, 48]. This constant normal stiffness K is defined as:

$$K = \frac{\dot{\sigma}_n}{\dot{\epsilon}_n} \tag{1}$$

where $\dot{\sigma}_n$ and $\dot{\epsilon}_n$ are the stress and strain increments normal to the interface. This constant normal stiffness condition is called the "confined dilatancy" condition (see [16]). The hypothesis is that the soil acts as a constant spring which confines the interface.

The commonly used framework for soil–structure interface modelling based on the elasto-plasticity theory was presented by Refs. [3, 6, 8, 15, 17, 18, 53]. Furthermore, various different modelling frameworks were proposed, e.g., damage models [26, 27], general plasticity formulations [31–33] and disturbed state concept by Refs. [14, 52].

In addition, the hypoplastic framework proposed by Gudehus [22] was used to simulate the contact behaviour of granular-solid interface. The hypoplasticity described by Gudehus [22] is based on the earlier developments from Kolymbas [29] and Wu [50]. The hypoplasticity formulation proposed by Wu and Bauer [51] was adapted, for the modelling of an infinite simple shear condition by Herle and Nübel [25]. This first hypoplastic interface model was followed, by Gutjahr [23], who developed a 1-D hypoplastic interface model from the hypoplasticity 3-D model with predefined limit state surface given by Von Wolffersdorff [49]. The model proposed by Gutjahr [23] was able to simulate different surface roughness conditions. Arnold and Herle [2] reformulated the hypoplastic model with a predefined limit surface [49] for 2-D interface conditions under the assumption of reduced stress and stretching tensors.

Weißenfels and Wriggers [46] developed a projection method to integrated plasticity models into a mixed mortar formulation. In opposite to that, the goal of our paper is the definition of an enhanced hypoplastic interface model, which can be implemented into existing numerical formulations, e.g., Refs. [4, 5, 14, 22].

In the following section, we give a brief description of the basic hypoplasticity formulations and tensorial notations. The interface model from Arnold and Herle [2] is introduced with the reduced stress and stretching tensors in Sect. 3. To this purpose, the reformulation of the tensorial operators is presented in Sect. 3.1. The reduced tensors are extended by the in-plane stresses at the interface, and an enhanced model is proposed (Sect. 4). The new stress and stretching tensors are used with modified tensorial operators to model the contact behaviour of the interfaces.

In Sect. 5, the enhanced model is validated against the model given by Arnold and Herle [2]. The different approaches modelling the surface roughness at the interface proposed by Arnold and Herle [2] and Gutjahr [23] are compared and examined in Sect. 6. The last validation is performed in Sect. 6.5 to compare the simulations of the enhanced model with existing experimental data found in the literature. Finally, the paper concludes with a short discussion about the benefits and limitations of the proposed model.

2 General tensorial and hypoplastic definitions

The general form of the hypoplastic model formulation [22] can be written as:

$$\dot{\boldsymbol{T}} = f_s(\boldsymbol{L} : \boldsymbol{D} + f_d \boldsymbol{N}||\boldsymbol{D}||) \tag{2}$$

where $\dot{\boldsymbol{T}}$ and $\boldsymbol{D}$ are the objective stress rate and stretching tensor, respectively. $\boldsymbol{N}$ and $\boldsymbol{L}$ are the fourth- and second-order constitutive tensors. f_s is the barotropy factor controlling the influence of the mean stress and f_d is the pyknotropy factor considering the influence of the relative density.

Von Wolffersdorff [49] extended the basic form of the model by incorporating a predefined limit state surface after Matsuoka and Nakai [36]. The second-order constitutive tensor $\boldsymbol{L}$ is then defined as:

$$\boldsymbol{L} = f_s \frac{1}{\hat{\boldsymbol{T}} : \hat{\boldsymbol{T}}} \left(F^2 \boldsymbol{I} + a^2 \hat{\boldsymbol{T}} \otimes \hat{\boldsymbol{T}}\right) \tag{3}$$

where $\hat{\boldsymbol{T}} = \boldsymbol{T}/\mathrm{tr}\boldsymbol{T}$ is a deviator stress and $\boldsymbol{I}$ is the fourth-order unity tensor. The coefficient a is defined as:

$$a = \frac{\sqrt{3}(3 - \sin\varphi_c)}{2\sqrt{2}\sin\varphi_c} \tag{4}$$

where φ_c is a model parameter. The Matsuoka–Nakai condition is given by the following scalar coefficient as:

$$F = \sqrt{\frac{1}{8}\tan^2\psi + \frac{2 - \tan^2\psi}{2 + \sqrt{2}\tan\psi\cos 3\theta}} - \frac{1}{2\sqrt{2}}\tan\psi \tag{5}$$

with the Lode angle θ,

$$\cos 3\theta = -\sqrt{6}\frac{\mathrm{tr}\left(\hat{\boldsymbol{T}}^* \cdot \hat{\boldsymbol{T}}^* \cdot \hat{\boldsymbol{T}}^*\right)}{\left[\hat{\boldsymbol{T}}^* : \hat{\boldsymbol{T}}^*\right]^{3/2}} \tag{6}$$

where $\hat{\boldsymbol{T}}^* = \hat{\boldsymbol{T}} - \frac{1}{3}\boldsymbol{I}$ is a deviator stresses and $\tan\psi = \sqrt{3}||\hat{\boldsymbol{T}}^*||$. The fourth-order constitutive tensor is defined as:

$$\boldsymbol{N} = f_s f_d \frac{a \cdot F}{\hat{\boldsymbol{T}} : \hat{\boldsymbol{T}}} \left(\hat{\boldsymbol{T}} + \hat{\boldsymbol{T}}^*\right) \tag{7}$$

The barotropy factor f_s controls the influence of the mean stress and is given as:

$$f_s = \frac{h_s}{n}\left(\frac{e_i}{e}\right)^{\beta}\frac{1+e_i}{e_i}\left(\frac{-\mathrm{tr}(\boldsymbol{T})}{h_s}\right)^{1-n}\cdot\left[3+a^2-a\sqrt{3}\left(\frac{e_{i0}-e_{d0}}{e_{c0}-e_{d0}}\right)^{\alpha}\right]^{-1} \tag{8}$$

The pyknotropy factor f_d controls the influence of the relative density, i.e.,

$$f_d = \left(\frac{e-e_d}{e_c-e_d}\right)^{\alpha} \tag{9}$$

where e_d, e_c, e_i are limiting void ratios. Under increasing mean pressure, they decrease until the limiting values e_{d0}, e_{c0}, e_{i0} are reached (see Fig. 1).

$$\frac{e_d}{e_{d0}} = \frac{e_c}{e_{c0}} = \frac{e_i}{e_{i0}} = \exp\left[-\left(\frac{\mathrm{tr}(\boldsymbol{T})}{h_s}\right)^{n}\right] \tag{10}$$

The model parameters are φ_c the critical state friction angle, the parameters h_s and n that control the normal compression lines and the critical state line. Furthermore, α controls the relative density to peak friction dependency and β controls the relative density to the soil stiffness dependency. Detailed information about the hypoplastic model with a predefined limit surface and the parameter determination of the model are given in Von Wolffersdorff [49] and Herle and Gudehus [24].

2.1 Shear zone thickness

The interface model is defined in a stress-strain space; therefore, the displacement at the interface has to be calculated for a given stretching and vice versa. Arnold and Herle [2] introduced the dependence of the shear zone thickness d_s on the shear strain γ_i to calculate the interface displacement u_i (see Fig. 2). The shear zone thickness is correlated with the mean grain size d_{50}. This thickness can vary between 5 and 10 times the mean grain size d_{50}. The experimental evidence of the shear zone thickness for granular assemblies was studied by Tejchman and Wu [43] using a plane strain device. Newer results from DeJong and Westgate [12], DeJong et al. [13] and Martinez et al. [34] confirm these results. The shear strain γ_i with $i \in \{x; z\}$ is given in terms of the shear displacement at critical state as:

$$\tan\gamma_i = \frac{u_i}{d_s} \tag{11}$$

d_s is influenced by the density, the mean grain size diameter d_{50} and the surface roughness. The exact choice of d_s is a priori difficult to determine. To this reason, d_s can be used from back–calculations as mentioned by Arnold and Herle [2].

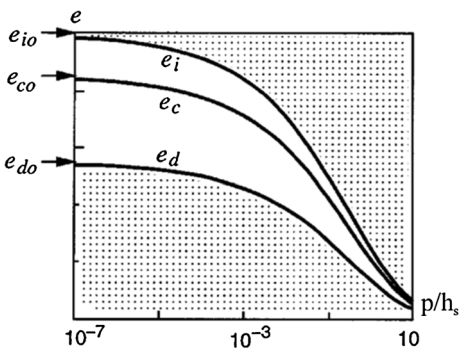

Fig. 1 Relation between e_d, e_c, e_i and p, from Herle and Gudehus [24]

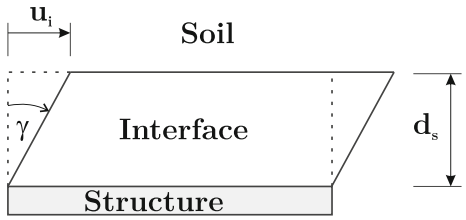

Fig. 2 Definition of the shear zone thickness and shear strain at critical state modified from Gutjahr [23]

3 Hypoplastic model for the interface behaviour

On the basis of the hypoplastic model of Von Wolffersdorff [49], a 2-D hypoplastic interface model was formulated by Arnold and Herle [2]. With the introduction of a reduced stress and stretching tensor assuming that the global axis is connected to the contact plane axis as $y||1$, $x||2$ and $z||3$, as shown in Fig. 3. The shear stress relations are defined as: $\sigma_{12} = \sigma_{21} = \tau_x$, $\sigma_{13} = \sigma_{31} = \tau_z$. The normal interface stress is the mean effective stresses in the y-direction $\sigma_{11} = \sigma_n$. Both other mean stresses are assumed to be $\sigma_{22} = \sigma_{33} = \sigma_n$. The out-of-plane shear stress is assumed to be $\sigma_{23} = 0$. This assumption is justified for the standard interface boundary condition of one rigid incompressible surface (e.g., piles, retaining walls or tunnel linings). The stress tensor $\boldsymbol{T}$ is:

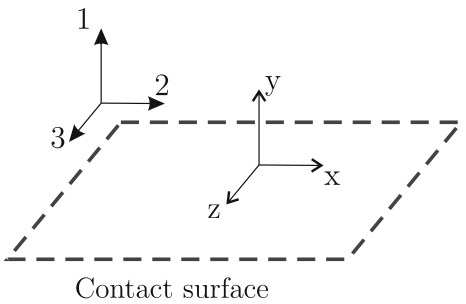

Fig. 3 Contact plane and coordinate system proposed by [2]

$$\boldsymbol{T}^{\mathrm{f}} = \begin{bmatrix} \sigma_{11} & \sigma_{12} & \sigma_{13} \\ \sigma_{21} & \sigma_{22} & \sigma_{23} \\ \sigma_{31} & \sigma_{32} & \sigma_{33} \end{bmatrix} \Rightarrow \boldsymbol{T} = \begin{bmatrix} \sigma_{\mathrm{n}} & \tau_x & \tau_z \\ \tau_x & \sigma_{\mathrm{n}} & 0 \\ \tau_z & 0 & \sigma_{\mathrm{n}} \end{bmatrix} \tag{12}$$

where $\boldsymbol{T}^{\mathrm{f}}$ denotes the full stress tensor and $\boldsymbol{T}$ denotes the reduced stress tensor. Considering the same assumptions as for the stress tensor, the stretching tensor $\boldsymbol{D}^{\mathrm{f}}$ is defined as:

$$\boldsymbol{D}^{\mathrm{f}} = \begin{bmatrix} \dot{\varepsilon}_{11} & \dot{\varepsilon}_{12} & \dot{\varepsilon}_{13} \\ \dot{\varepsilon}_{21} & \dot{\varepsilon}_{22} & \dot{\varepsilon}_{23} \\ \dot{\varepsilon}_{31} & \dot{\varepsilon}_{32} & \dot{\varepsilon}_{33} \end{bmatrix} \Rightarrow \boldsymbol{D} = \begin{bmatrix} \dot{\varepsilon}_{\mathrm{n}} & \frac{\dot{\gamma_x}}{2} & \frac{\dot{\gamma_z}}{2} \\ \frac{\dot{\gamma_x}}{2} & \dot{\varepsilon}_{\mathrm{n}} & 0 \\ \frac{\dot{\gamma_z}}{2} & 0 & \dot{\varepsilon}_{\mathrm{n}} \end{bmatrix} \tag{13}$$

Arnold and Herle [2] used the reduced stress and stretching tensors to derive the interface hypoplastic model. Note that here we do not follow Arnold and Herle [2] notation. Instead, we express their model using notation adopted in this paper.

The first and second entry of the stress vector is the stress normal to the interface σ_{n}. These are assumed to be equal. The shear stresses are $\sigma_{12} = \sigma_{21} = \tau_x$ and $\sigma_{13} = \sigma_{31} = \tau_y$, whereas, the third shear stress is $\sigma_{23} = \sigma_{32} = 0$. This is not used in the vectorial notation. The definitions for the reduced stress and stretching vectors are:

$$\boldsymbol{T} = \begin{bmatrix} \sigma_{\mathrm{n}} \\ \sigma_{\mathrm{n}} \\ \tau_x \\ \tau_z \end{bmatrix} \tag{14}$$

where σ_{n} is the stress normal to the interface and τ_x, τ_z are the shear stresses. The stretching vector is written as:

$$\boldsymbol{D} = \begin{bmatrix} \dot{\epsilon_{\mathrm{n}}} \\ \dot{\epsilon_{\mathrm{n}}} \\ \frac{\dot{\gamma_x}}{2} \\ \frac{\dot{\gamma_z}}{2} \end{bmatrix} \tag{15}$$

where $\dot{\epsilon_{\mathrm{n}}}$ is the stretching rate normal to the interface and $\frac{\dot{\gamma_x}}{2}$, $\frac{\dot{\gamma_z}}{2}$ are the shear stretching rates in the x- and z-directions. These tensors are used within modified tensorial operators given in Sect. 3.1. The modified tensorial notation is used with the standard formulation of the hypoplastic model after Von Wolffersdorff [49]. This leads to the model proposed by Arnold and Herle [2]. Beside these modifications to the original model, different terms are used in the interface model by Arnold and Herle [2]. The influence of these modifications is discussed later. The Lode angle is assumed to be $\cos 3\theta = 0$. The Matsuoka–Nakai stress factor is given by Arnold and Herle [2] as:

$$F = \sqrt{1 - \frac{9}{4}\left(\left(\frac{\tau_x}{3\sigma}\right)^2 + \left(\frac{\tau_z}{3\sigma}\right)^2\right)} - \frac{\sqrt{3}}{2}\sqrt{\left(\frac{\tau_x}{3\sigma}\right)^2 + \left(\frac{\tau_z}{3\sigma}\right)^2} \tag{16}$$

In addition, Arnold and Herle [2] proposed a modified coefficient a following the suggestion of Herle and Nübel [25] that the correct behaviour of the interface zone at critical state can be modelled by:

$$a = 3\sqrt{\frac{1}{2\tan^2\psi} - \frac{1}{8}} - \frac{\sqrt{3}}{2\sqrt{2}} \tag{17}$$

It is assumed that under uni-axial shearing in the x-direction the shear stress $\tau_z = \dot{\gamma}_z/2 = 0$ vanishes.

The hypoplastic interface model proposed by Arnold and Herle [2] has several shortcomings, in particular, the in-plane stress σ_{p} and in-plane stretching ε_{p} are not incorporated in the model formulation. The consequence of neglecting the in-plane stresses is the assumption of an isotropic stress state at the interface.

3.1 General definitions for new operators

The idea of our modelling approach is as follows: we preserve the formulation of the continuum constitutive models, but redefine the tensorial operators so that in combination with the reduced stress [Eq. (14)] and stretching vectors [Eq. (15)] the models correctly simulate the interface behaviour.

The *Voigt* notation is used to reduce the second-order and fourth-order tensors into vectors and matrices. We define the first-rank tensors $\boldsymbol{X}$ and $\boldsymbol{Y}$ and the second-rank tensor $\mathcal{S}$ is introduced as:

$$\boldsymbol{X} = \begin{bmatrix} X_1 \\ X_2 \\ X_3 \\ X_4 \end{bmatrix} \quad \boldsymbol{Y} = \begin{bmatrix} Y_1 \\ Y_2 \\ Y_3 \\ Y_4 \end{bmatrix} \quad \mathcal{S} = \begin{bmatrix} S_{11} & S_{12} & S_{13} & S_{14} \\ S_{21} & S_{22} & S_{23} & S_{24} \\ S_{31} & S_{32} & S_{33} & S_{34} \\ S_{41} & S_{42} & S_{43} & S_{44} \end{bmatrix} \tag{18}$$

The Euclidean norm of $\boldsymbol{X}$ is the written as:

$$||\boldsymbol{X}|| = \sqrt{X_1^2 + 2X_2^2 + 2X_3^2 + 2X_4^2} \tag{19}$$

The trace of $\boldsymbol{X}$ is defined as:

$$\mathrm{tr}(\boldsymbol{X}) = \mathrm{X}_1 + 2\mathrm{X}_2 \tag{20}$$

The determinant from $\boldsymbol{X}$ is defined as:

$$\det(\boldsymbol{X}) = X_1X_2^2 - X_4^2X_2 - X_3^2X_2 \tag{21}$$

The second-order unity tensor as used in the vectorial notation is:

$$\boldsymbol{I} = \begin{bmatrix} 1 \\ 1 \\ 0 \\ 0 \end{bmatrix} \tag{22}$$

and the fourth-order unity tensor is:

$$\boldsymbol{I} = \begin{bmatrix} 1 & 0 & 0 & 0 \\ 0 & 0.5 & 0 & 0 \\ 0 & 0 & 0.5 & 0 \\ 0 & 0 & 0 & 0.5 \end{bmatrix} \tag{23}$$

The deviator stress $\boldsymbol{X}^*$ is given as:

$$\hat{\boldsymbol{X}} = \frac{\boldsymbol{X}}{\mathrm{tr}\boldsymbol{X}} = \begin{bmatrix} \frac{X_1}{X_1 + 2X_2} \\ \frac{X_2}{X_1 + 2X_2} \\ \frac{X_3}{X_1 + 2X_2} \\ \frac{X_4}{X_1 + 2X_2} \end{bmatrix} \tag{24}$$

The deviator stress $\hat{\boldsymbol{X}}^*$ is defined in vectorial notation:

$$\hat{\boldsymbol{X}}^* = \frac{\boldsymbol{X}}{\mathrm{tr}\boldsymbol{X}} - \frac{\boldsymbol{I}}{3} = \begin{bmatrix} \frac{X_1}{X_1 + 2X_2} - \frac{1}{3} \\ \frac{X_2}{X_1 + 2X_2} - \frac{1}{3} \\ \frac{X_3}{X_1 + 2X_2} \\ \frac{X_4}{X_1 + 2X_2} \end{bmatrix} \tag{25}$$

The inner product $(\cdot)$ is formulated as:

$$\boldsymbol{X} \cdot \boldsymbol{Y} = \begin{bmatrix} X_1Y_1 + X_3Y_3 + X_4Y_4 \\ X_2Y_2 + X_3Y_3 \\ X_1Y_3 + X_3Y_2 \\ X_4Y_1 + X_2Y_4 \end{bmatrix} \tag{26}$$

The double inner product $(:)$ between two first-rank tensors is defined as:

$$\boldsymbol{X} : \boldsymbol{Y} = X_1Y_1 + 2X_2Y_2 + 2X_3Y_3 + 2X_4Y_4 \tag{27}$$

The double inner product $(:)$ between second-rank and first-rank tensors is given as:

$$\mathcal{S} : \boldsymbol{Y} = \begin{bmatrix} S_{11}Y_1 + 2S_{12}Y_2 + 2S_{13}Y_3 + 2S_{14}Y_4 \\ S_{21}Y_1 + 2S_{22}Y_2 + 2S_{23}Y_3 + 2S_{24}Y_4 \\ S_{31}Y_1 + 2S_{32}Y_2 + 2S_{33}Y_3 + 2S_{34}Y_4 \\ S_{41}Y_1 + 2S_{42}Y_2 + 2S_{43}Y_3 + 2S_{44}Y_4 \end{bmatrix} \tag{28}$$

Also, the outer product $(\otimes)$ is defined as:

$$\boldsymbol{X} \otimes \boldsymbol{Y} = \begin{bmatrix} X_1Y_1 & X_1Y_2 & X_1Y_3 & X_1Y_4 \\ X_2Y_1 & X_2Y_2 & X_2Y_3 & X_2Y_4 \\ X_3Y_1 & X_3Y_2 & X_3Y_3 & X_3Y_4 \\ X_4Y_1 & X_4Y_2 & X_4Y_3 & X_4Y_4 \end{bmatrix} \tag{29}$$

The redefined tensorial operators are used with the reduced stress and stretching tensors for the modelling of the interface behaviour. The enhancement of the interface model is described in the following section.

4 Enhancement of the hypoplastic contact model

As outlined in the previous section, the hypoplastic interface model by Arnold and Herle [2] will be enhanced. A study of the model formulation leads to the understanding that the stress tensor entries $\sigma_{22} = \sigma_{33}$, assumed to be equal to normal contact stress σ_n, is not valid. To improve the model predictions, the reduced stress and stretching tensor are redefined as:

$$\boldsymbol{T} = \begin{bmatrix} \sigma_\mathrm{n} & \tau_x & \tau_z \\ \tau_x & \sigma_\mathrm{p} & 0 \\ \tau_z & 0 & \sigma_\mathrm{p} \end{bmatrix} \tag{30}$$

where σ_n is the stress normal to the interface and σ_p are the in-plane stress components. The same modification is done with the stretching tensor $\boldsymbol{D}$ where the strains $\varepsilon_{22} = \varepsilon_{33} = 0$. The modified stretching tensor has the following form:

$$\boldsymbol{D} = \begin{bmatrix} \dot{\varepsilon}_\mathrm{n} & \frac{\dot{\gamma_x}}{2} & \frac{\dot{\gamma_z}}{2} \\ \frac{\dot{\gamma_x}}{2} & 0 & 0 \\ \frac{\dot{\gamma_z}}{2} & 0 & 0 \end{bmatrix} \tag{31}$$

The new defined stress and stretching tensors are shown in Fig. 4. As modification to the stress vector used in the model by Arnold and Herle [2] the in-plane stress $\sigma_\mathrm{p} = \sigma_{22} = \sigma_{33}$ are used. These are assumed to be constant. In vectorial notation the stress tensor are:

$$\boldsymbol{T} = \begin{bmatrix} \sigma_\mathrm{n} \\ \sigma_\mathrm{p} \\ \tau_x \\ \tau_z \end{bmatrix} \tag{32}$$

Instead of the assumption from Arnold and Herle [2] the stretching tensor is defined as:

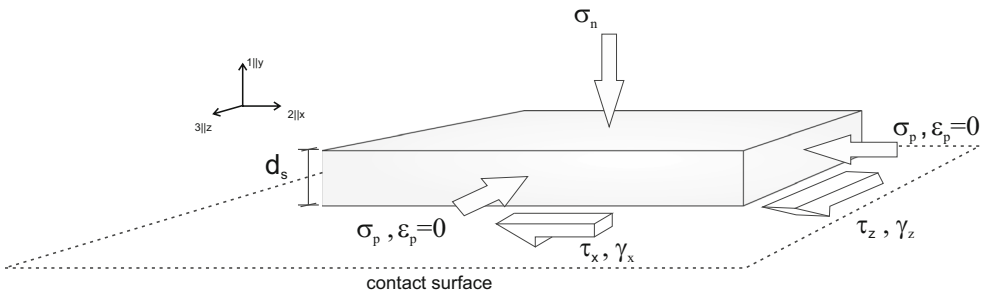

Fig. 4 Illustration of the enhanced defined reduced stress and stretching tensor at element level

$$\boldsymbol{D} = \begin{bmatrix} \dot{\varepsilon}_{\mathrm{n}} \\ 0 \\ \frac{\dot{\gamma_x}}{2} \\ \frac{\dot{\gamma_z}}{2} \end{bmatrix} \tag{33}$$

The modified reduced tensors are used to establish the enhanced model for hypoplastic granular interfaces. The modification is a consequence of the assumption of an oedometric condition at the interface under an applied normal load, whereas the original model by Arnold and Herle [2] assumed an isotropic stress state at the interface. Furthermore, the in-plane stress σ_{p} can develop separately from the normal stress σ_{n} under shear conditions. Table 1 shows the equivalent tensor to vector indices for the notation used by Arnold and Herle [2] (AH model) and the enhanced model (AHE model).

The hypoplastic model with predefined critical state conditions, proposed by Von Wolffersdorff [49] is used with the modified tensorial operators given in Sect. 3.1 and the stress [Eq. (32)] and stretching [Eq. (33)] vectors. The model uses the same hypoplastic parameters as described in Sect. 2.

Note that unlike the model from Sect. 3, the enhanced interface model simulates an identical response for drained simple shear simulations and oedometric test in comparison with the full 3-D hypoplastic model.

In the following, a comparison of different models is conducted. Two different model formulations without the extended reduced stress and stretching tensors are used. First, the model proposed by Arnold and Herle [2] and then an enhanced basic model by Arnold and Herle [2] are defined. The latter uses the following differences compared to the published model of Arnold and Herle [2]:

- The Lode angle assumption in the model of Arnold and Herle [2] is corrected, i.e. $\cos 3\theta \neq 0$
- The standard definition of the coefficient a [see Eq. (4)] is used
- The Matsuoka-Nakai stress factor F from the original model from the model of Von Wolffersdorff [49] is used [Eq. (5)]

In the following, the three models are abbreviated as:

- Model proposed by Arnold and Herle [2]: AH
- Model based on the definition of Arnold and Herle [2] enhanced by using $\cos 3\theta$, a and F from the 3-D continuum model: AHE
- Enhanced model with $\kappa_{\mathrm{r}} = 1.0$ proposed in this paper: HvWE

Table 1 Indices for the full and reduced tensorial notation

Tensor index	Vector index AH model	Vector index AHE model	Symbolic index AHE model
11	1	1	n
22/33	1	2	p
12/21	2	3	x
13/31	3	4	z
23/32	–	–	–

4.1 Remarks on the numerical implementation

The numerical implementation of the enhanced stress assumption is done by the introduction of σ_{p} as additional state variable. The in-plane stresses are not used in different numerical approaches as: zero-thickness interface elements [4], mortar-methods [5] or thin-layer interface elements [14].

The initialization of the state variable should be done before the first shearing deformation occurs. The expected value for the in-plane stress can be calculated using the Jaky formula [28].

The Euler stretching tensor is calculated as the symmetric part of velocity gradient, and the objective Jaumann–Zaremba stress rate as the time-derivative of the stress tensor corrected for rotations, as standard in continuum mechanics. Their calculation is a matter of the finite element code where the interface model is to be used and it is outside the scope of the present paper.

5 Evaluation of the models

The enhanced model (HvWE) proposed in the previous section is compared to the model from Arnold and Herle [2] (AH) and the slightly modified model (AHE). The validation is done using the three common boundary conditions for soil–structure interfaces, which are defined as (see [15]):

- Constant volume (CV):

$K = \infty; \dot{\sigma} \neq 0; \dot{\varepsilon} = 0$

- Constant normal load (CNL) :

$K = 0; \dot{\sigma} = 0; \dot{\varepsilon} \neq 0$

- Constant normal stiffness (CNS) :

$K = \text{constant}; \dot{\sigma} \neq 0; \dot{\varepsilon} \neq 0$

where the stiffness K is introduced by Eq. (1). The constant volume and the constant normal load are referred as the upper and lower limits in interface testing. Detailed information about the difference in the test conditions is given in Costa D'Aguiar et al. [9]. The constant normal stiffness condition refers to the in situ state for interface testing. The granular interface models are validated against each other using these three boundary conditions.

The parameters for the Hostun sand used in the simulation are given in Table 2. The stress path for the CV tests is shown in Figs. 5 and 6. Our initial void ratio in all CV simulations is $e_0 = 0.8$. The proposed model (HvWE) gives the lowest shear stress τ_x at different normal stress levels. The models have the same trend but the shear stress obtained varies. The original model (AH) leads to the highest shear stresses. The AHE and HvWE models show a small difference in their response. At a higher normal stress, the model responses show significant differences. Similar observations are seem for the τ_x–σ_n results shown in Fig. 6. The difference between the HvWE and AHE model is small compared to the AH model. The predicted normal stresses are higher for the AH than for the AHE model.

The results from the CNS comparison are given in Figs. 7 and 8. The applied constant normal stiffness is 1000 kPa. The initial void ratio applied in the CNS and CNL simulations is $e_0 = 0.65$. The applied normal stress varies from 50 to 150 kPa.

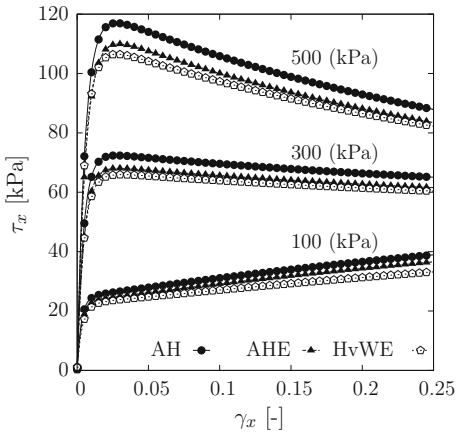

Fig. 5 τ_x–γ_x stress path for the comparison of different models under CV conditions with 100, 300 and 500 kPa applied normal stress

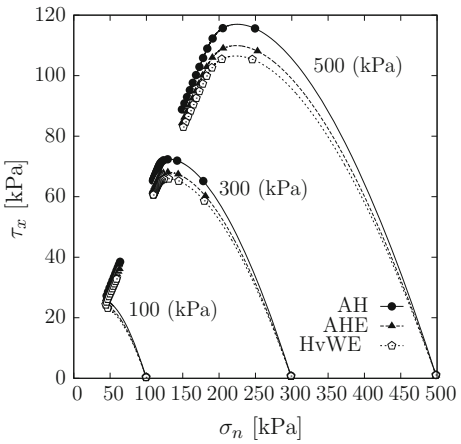

Fig. 6 τ_x–σ_n stress path for the comparison of different models under CV conditions with 100, 300 and 500 kPa applied normal stress

The shear behaviour is similar in all models, see Fig. 7. However, the HvWE model shows the largest shear stress at all different applied normal stress levels.

Figure 8 shows the behaviour in the σ_n–τ_x plane. It can be observed that the resulting normal stress in the HvWE model differs significantly from the stress paths obtained using the Arnold and Herle [2] model.

The last model comparison is done under a constant normal load (CNL) condition. This condition is characterised by $\dot{\sigma}_n = 0$ and $\dot{\varepsilon}_n \neq 0$. Figure 9 shows the results for

Table 2 Parameters for the hypoplastic model (partly from Herle and Gudehus [24])

	φ_c (°)	h_s (MPa)	n	e_{d0}	e_{c0}	e_{i0}	α	β
Hostun sand	31	1000	0.29	0.61	0.96	1.09	0.13	2
Toyura sand	30	2600	0.27	0.61	0.98	1.10	0.25	1
Ticino sand	31	1000	0.29	0.61	0.96	1.09	0.13	2
Density sand	32	750	0.25	0.62	0.97	1.06	0.13	1.5

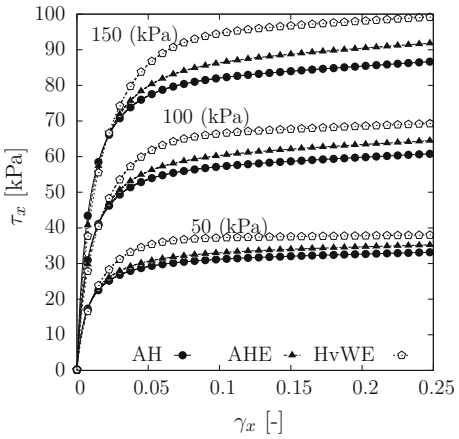

Fig. 7 γ_x–τ_x stress path for the comparison of different models under CNS conditions

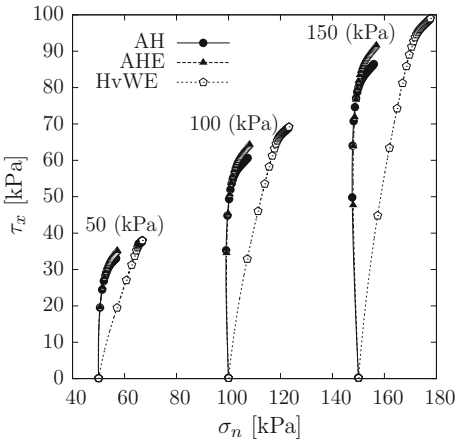

Fig. 8 τ_x–σ_n stress path for the comparison of different models under CNS conditions

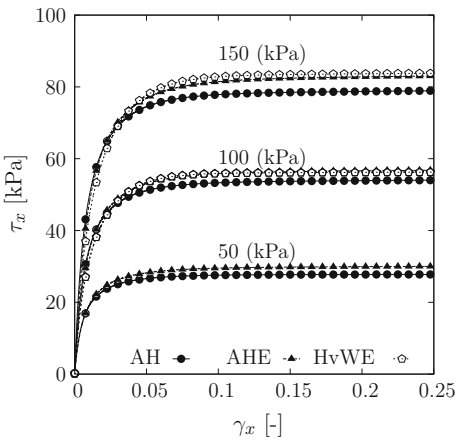

Fig. 9 τ_x–γ_x stress path for the comparison of different models under CNL conditions

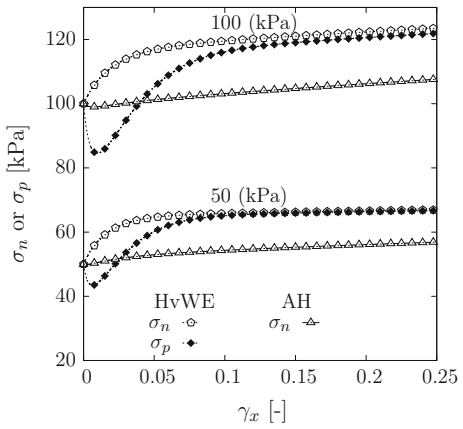

Fig. 10 Comparison of σ_n and the in-plane σ_p normal stress at the interface for the different models

the γ_x–τ_x graph. All three models have small differences in their response. Compared to the CNS stress path (see Fig. 7), lower shear stresses develop under CNL conditions.

As a summary, all three models (AH, AHE and HvWE) give different model responses.

5.1 Discussion of model behaviour

The behaviour of the different models differs in several aspects. The first aspect is the proposed coefficient a, the factor of the Matsuoka–Nakai failure criterion F and the lode angle $\cos 3\theta = 0$ from Arnold and Herle [2] which explains the difference between the AH and AHE model. The differences between the AH, AHE and the model that we proposed (HvWE) is associated with the in-plane stress σ_p. To demonstrate this behaviour, Fig. 10 shows the normal stress and in-plane stress development under CNS conditions for the AH and HvWE models.

Figure 10 highlights the significant effect of the in-plane stresses in the simulations. The following section introduces and compares the two different approaches to incorporate the surface roughness into the proposed enhanced interface model.

6 Modelling the interface behaviour with various roughnesses

The models introduced in the previous Sects. 3 and 4 use the assumption of fully rough conditions. As indicated in Refs. [11, 30, 44], the surface roughness is particularly important to the interface shear behaviour. Therefore, Gutjahr [23] and Arnold and Herle [2] introduced different approaches to model the surface roughness.

To demonstrate their differences and equalities the notation is adjusted from the original publications.

6.1 Surface roughness approach after Gutjahr [23]

Gutjahr [23] used the parameter κ_r to describe the contact surface roughness. This parameter κ_r can be estimated by the empirical formula:

$$\kappa_r = 0.25 \log R_n + 1.05 \leq 1 \tag{34}$$

where R_n is the normalised roughness. Thus, R_n depends on the surface roughness R and the mean grain size d_{50} as introduced by Uesugi and Kishida [44]. Gutjahr [23] proposed another way of determining the parameter κ_r as:

$$\kappa_r = \tan \varphi_{int} / \tan \varphi_c \leq 1.0 \tag{35}$$

where φ_{int} is the interface friction angle. This definition describes the relationship between the soil–soil friction angle and the interface friction angle φ_{int}. Gutjahr [23] suggested that the existing surface roughness will alter the pyknotropy factor f_d and the critical state friction angle φ_c. The scalar function of a [see Eq. (4)] is influenced by φ_c. Therefore, Gutjahr [23] proposed a new definition of a as:

$$a_r = \frac{1}{\kappa_r \varphi_c} \tag{36}$$

Based on their results, Uesugi and Kishida [44] concluded that loose soil on rough surfaces has the same behaviour as dense soil on smooth surfaces. Thus, Gutjahr [23] proposed a new pyknotropy factor f_d as:

$$f_{dr} = \left(\frac{e - e_d}{e_c - e_d} \right)^{\alpha \kappa_r^2} \tag{37}$$

followed by a modification of the barotropy factor f_s as:

$$f_{sr} = \frac{h_s}{n} \left(\frac{e_i}{e} \right)^{\beta} \frac{1 + e_i}{e_i} \left(\frac{-\mathrm{tr}(\boldsymbol{T})}{h_s} \right)^{1-n} \cdot \left[3 + a_r^2 - a_r \sqrt{3} \left(\frac{e_{i0} - e_{d0}}{e_{c0} - e_{d0}} \right)^{\alpha \kappa_r^2} \right]^{-1} \tag{38}$$

These modifications are used in the formulation of the $\boldsymbol{L}$-Tensor and the $\boldsymbol{N}$-Tensor by replacing a, f_d and f_s by a_r, f_{dr} and f_{sr}

6.2 Surface roughness approach after Arnold and Herle [2]

Arnold and Herle [2] proposed a different scheme to model various surface roughnesses in the hypoplastic interface model. Here, the scalar value a is modified in the same way as Gutjahr [23]. However, Arnold and Herle [2] adjusted the mobilisation of the shear stress by introducing the additional coefficient f_c as:

$$f_c = \frac{1}{\kappa_r} \tag{39}$$

Arnold and Herle [2] stated that this modification leads to better predictions when compared to experimental results. The additional coefficient f_c is a modification of the barotropy factor and is implemented into the general form of the hypoplastic equation [Eq. (2)] as:

$$\dot{\boldsymbol{T}} = f_s f_c (\boldsymbol{L} : \boldsymbol{D} + f_d \boldsymbol{N} ||\boldsymbol{D}||) \tag{40}$$

6.3 Comparison of the surface roughness modelling

In the following section, the two surface roughness approaches from Sects. 6.1 to 6.2 are evaluated. The parameters for Toyoura Sand from Table 2 are used in a constant normal load simulation. The results of the γ_x–τ_x graph are shown in Fig. 11. Both schemes for modelling the surface roughness are implemented into the enhanced hypoplastic interface model (HvWE) given in Sect. 4. The CNL simulations are undertaken with an applied normal initial stress of 100 kPa. As expected for $\kappa_r = 1.0$, both schemes give identical results. Using lower surface roughness coefficients $\kappa_r \leq 1.0$, the approach of Gutjahr [23] shows a softer response compared to that of Arnold and Herle [2]. Figure 12 shows the shear strain γ_x –normal strain ε_n graph. The results demonstrate that the scheme by Arnold and Herle [2] has less influence on the normal behaviour, whereas the scheme by Gutjahr [23] for fully rough conditions shows a dilative behaviour. Using $\kappa_r = 0.45$ for a smoother surface, after initial compaction a minor dilative behaviour is calculated. All simulations use an initial void ratio of $e_0 = 0.6$.

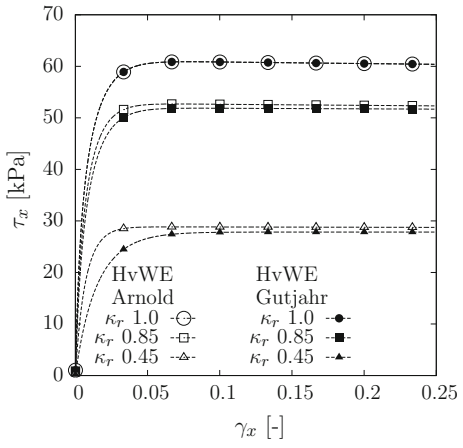

Fig. 11 CNL simulation of the two different surface roughness modelling frameworks in the γ_x–τ_x plot

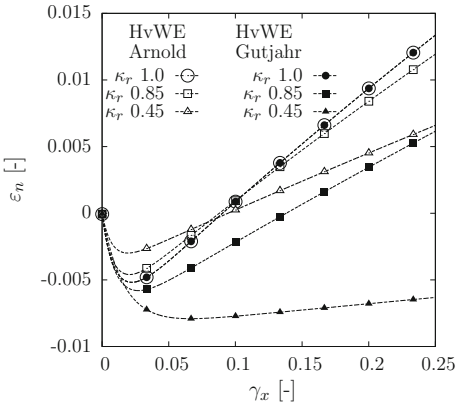

Fig. 12 CNL simulation of the two different surface roughness modelling schemes in the γ_x–ε_x plot

6.4 Modelling of surface roughness compared with experimental data

The enhanced model (HvWE) is used with the both surface roughness approaches. The experimental set-up is described in Uesugi and Kishida [44] and Uesugi et al. [45] using a modified direct shear test. The material tested was Toyorua sand, and the parameters are given in Table 2. The surfaces of the test apparatus were constructed from mild steel, and the predefined surface roughness was measured. Figure 13 shows the shear displacement u_x– friction coefficient τ_x/σ_n. Both schemes and the experimental data give similar responses for smooth interface conditions ($\kappa_r = 0.21$). For intermediate surface roughness ($\kappa_r = 0.66$), the scheme by Gutjahr [23] shows a slightly better model response than the scheme by Arnold and Herle [2].

Considering rough surface conditions ($\kappa_r = 0.98$), the simulation and experimental results differ, with the approach by Gutjahr [23] being able to simulate the peak behaviour. The surface modelling approach by Arnold and Herle [2] simulates only a small peak behaviour. After reaching the peak stress, the simulations for both approaches tend to the same residual stress at critical state. The simulations show a similar shear stress to the values obtained values from the experiments (see Fig. 13).

As a result of this comparison of the two schemes, we recommend the use of the one by Gutjahr [23] to model surface roughness.

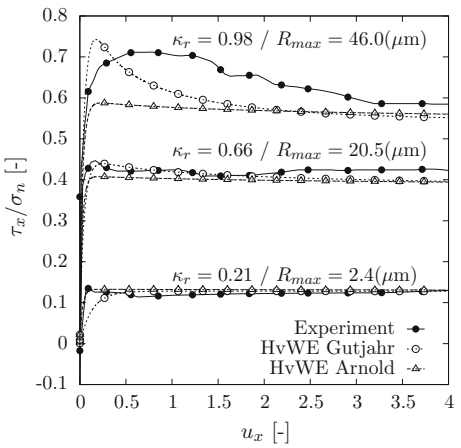

Fig. 13 shear displacement u_x—friction coefficient τ_x/σ_n plot for different surface roughness under CNL conditions with $\sigma_0 = 78$ kPa

6.5 Advanced verification of the proposed HvWE model

The first verification using experimental data is from a CNL test conducted with Hostun Sand (parameters are given in Table 2). The applied normal stress was 300 kPa, and the experiments were conducted on sand in a dense ($e_0 = 0.68$) and loose ($e_0 = 0.95$) state. The structural interface in these both experiments were fully rough ($\kappa_r = 1.0$). Figure 14 shows the shear displacement u_x–shear stress τ_x graph. The comparison shows that neither model matches with the experimental observations. Nevertheless, the proposed model HvWE gives a more accurate prediction than the AH model.

The next verification is done by using staged shear stress paths. This is defined by Gómez et al. [19] as stress path with fluctuating normal stress under continuously applied shear displacement. Gómez et al. [20] show that such a stress path can occur at the walls of navigation locks. In Fig. 15 a staged shear test is shown. The parameters used for the comparison are given in Table 2. The initial void ratio is taken according to the experimental set-up (see [19]) i.e., $e_0 = 0.68$. The roughness of the interface is assumed to be fully rough ($\kappa_r = 1.0$)

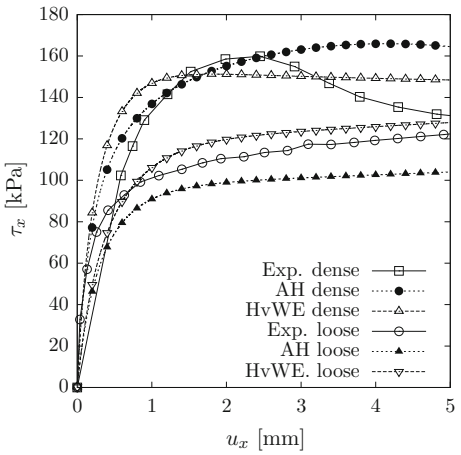

Fig. 14 Comparison of models of CNL test under an applied normal stress of 300 kPa using the experimental data by Shahrour and Rezaie [41]

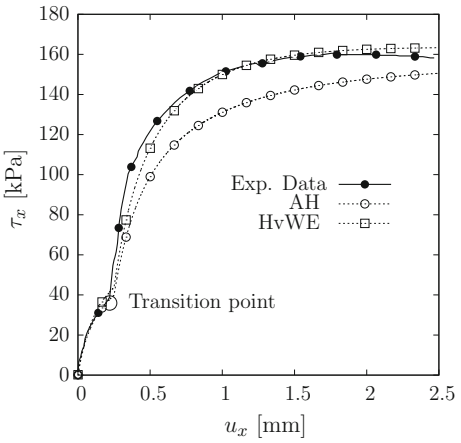

Fig. 15 Comparison of AH and HvWE models with the experimental data of a staged shear test under CNL conditions (102–274 kPa)

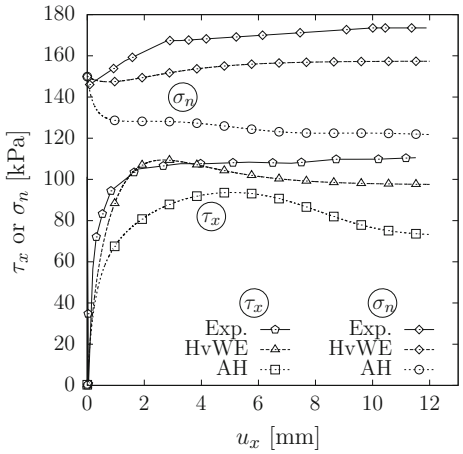

Fig. 16 Comparison of shear displacement u_x—shear stress τ_x and normal stress σ_n using experimental data with $K = 100$ kPa from Porcino et al. [39]

The experimental data [19] are compared with the AH and HvWE models. The transition point in Fig. 15 denotes the normal stress change in the test. Initially, a normal stress of 102 kPa is applied at the interface. When the shear displacement reaches 0.25 mm, the applied normal stress is increased to 274 kPa. The HvWE gives results similar to those of experimental data. The AH model has an identical response until the transition point, after which the simulated shear stress no longer coincides with the experimental results. This comparison highlights the enhanced predictive capability of the proposed HvWE model when in-plane stresses are considered.

The last verification is done using existing experimental data from Porcino et al. [39]. The parameters used are shown for the Ticino sand in Table 2. The interface used in the test was a rough aluminium interface, and the assumed surface roughness coefficient is assumed as $\kappa_r = 0.97$. Detailed information of the sand properties and parameters can be found in Herle and Gudehus [24].

Porcino et al. [39] conducted, CNS-tests in a modified direct shear apparatus to investigate different types of sand under changing normal stiffness conditions and varying interface roughness. The results are shown in Fig. 16. The shear behaviour of the HvWE model shows a similar behaviour to the experimental results. After the peak, the HvWE model experiences a softening, which was not observed in the experiments. The AH model also shows a strong softening in the model response and the shear stress at the critical state is underestimated.

The normal behaviour of the models show that the AH model exhibits contractive behaviour instead of dilative behaviour. The HvWE model simulates a small contractive state followed by continued shearing to dilative behaviour. Neither model matches the experimental observation; however, the HvWE model demonstrates a better behaviour than the AH model.

7 Conclusion

An enhanced model for the granular–solid interface is postulated on the basic hypoplastic 3-D continuum model from Von Wolffersdorff [49]. The three different models used in the comparison are:

- Basis hypoplastic interface granular model proposed by Arnold and Herle [2] (see Sect. 3)
- Basis hypoplastic interface granular model from Arnold and Herle [2] using the standard components from the 3-D continuum model (see Sect. 3)
- Enhanced hypoplastic granular interface model developed in this paper (see Sect. 4)

The enhancement is incorporated by defining new reduced stress and stretching tensors. These incorporate the in-plane stresses σ_p and in-plane strains $\varepsilon_p = 0$. By using the redefined tensorial operators given in the Sect. 3.1 and the reduced stress and stretching tensors the standard tensorial definitions (Sect. 2) give an enhanced model formulation for the interface.

Two different schemes for modelling the surface roughness are examined using experimental data and their formulations discussed. The enhanced model uses the approach proposed by Gutjahr [23] for modelling various surface roughnesses. The approach by Gutjahr [23] seems to give better predictions than the approach of Arnold and Herle [2].

The predictions obtained from the proposed model (HvWE) were better than the model response from the

Arnold and Herle [2] model. This was demonstrated by the comparison of the CNL test for loose and dense sand from Shahrour and Rezaie [41], the staged shear test using the experimental data of Gómez et al. [20] and the CNS test using the data of Porcino et al. [39].

The new enhanced model will contribute to the possibility of using the constitutive framework from the structure to the soil. The benefit is the use of the already calibrated model parameters from the surrounding soil and for the interface modelling. In addition, considering the reduced stress and strain notation is reducing the CPU load. The limitation of the enhanced model is that only monotonic stress paths can be modelled. The authors expect that better predictions can result from an improved parameter calibration. The application range of the presented approach is the presumption of a known contact geometry, in opposite to the method proposed by Weißenfels and Wriggers [47].

Anticipated future work will evaluate the use of the inter-granular strain concept of Niemunis and Herle [37] using the stress and stretching tensors given in Eqs. (32) and (33). This can be conducted on the basis of the work from Arnold [1] which applies the inter-granular strain concept to model interfaces using hypoplasticity.

Acknowledgments The first author greatly appreciates financial support by the German Research Foundation in the framework of the research training group 1462. The second author greatly appreciates financial support by the research Grant 15-05935S of the Czech Science Foundation.

References

1. Arnold M (2008) Application of the intergranular strain concept to the hypoplastic modelling of non-adhesive interfaces. In: The 12th international conference of International Association for Computer Methods and Advances in Geomechanics (IACMAG), pp 747–754
2. Arnold M, Herle I (2006) Hypoplastic description of the frictional behaviour of contacts. In: Schweiger HF (ed) Numerical methods in geotechnical engineering, sixth European conference on numerical methods in geotechnical engineering. Taylor & Francis, Graz, pp 101–106
3. Aubry D, Modaressi A, Modaressi H (1990) A constitutive model for cyclic behaviour of interfaces with variable dilatancy. Comput Geotech 9:47–58
4. Beer G (1985) An isoparametric joint/interface element for finite element analysis. Int J Numer Anal Methods Geomech 21:585–600
5. Belgacem F, Hild P, Laborde P (1998) The mortar finite element method for contact problems. Math Comput Model 28(4–8):263–271
6. Boulon M, Nova R (1990) Modelling of soil structure interface behavior a comparison between elastoplastic and rate type laws. Comput Geotech 9:21–46
7. Brumund W, Leonards GA (1973) Experimental study of static and dynamic friction between sand and typical construction material. J Test Eval 1(February):162–165
8. Clough GW, Duncan JM (1971) Finite element analyses of retaining wall behaviour. J Soil Mech Found Div 12:1657–1673
9. Costa DAguiar S, Modaressi A (2011) Piles under cyclic axial loading: study of the friction fatigue and its importance in pile behavior. Can Geotech J 48(10):1537–1550
10. Day R, Potts D (1998) The effect of interface properties on retaining wall behaviour. Int J Numer Anal Methods Geomech 22(February):1021–1033
11. De Jong JT, Randolph MF, White DJ (2003) Interface load transfer degradation during cyclic loading: a microscale investigation. Soils Found 43(4):81–93
12. DeJong JT, Westgate ZJ (2009) Role of initial state, material properties, and confinement condition on local and global soil–structure interface behavior. J Geotech Geoenviron Eng 135(11):1646–1660
13. DeJong JT, White DJ, Randolph M (2006) Microscale observation and modeling of soil-structure interface behavior using particle image velocimetry. Soils Found 46(1):15–28
14. Desai CS, Zaman MM, Lightner JG, Siriwardane HJ (1984) Thin-layer element for interfaces and joints. Int J Numer Anal Methods Geomech 8:19–43
15. Evgin E, Fakharian K (1996) Effect of stress paths on the behaviour of sandsteel interfaces. Can Geotech J 33:853–865
16. Fioravante V, Ghionna VN, Pedroni S, Porcino D (1999) A constant normal stiffness direct shear box for soil–solid interface tests. Riv Ital Geotec 3:7–22
17. Gennaro V, Frank R (2002) Elasto-plastic analysis of the interface behaviour between granular media and structure. Comput Geotech 29(7):547–572
18. Ghionna VN, Mortara G (2002) An elastoplastic model for sand–structure interface behaviour. Géotechnique 52(1):41–50
19. Gómez JE (2000) Development of an extended hyperbolic model for concrete-to-soil interfaces. Ph.D. thesis, Virginia Polytechnic Institute and State University
20. Gómez JE, Filz GM, Ebeling RM (2003) Extended hyperbolic model for sand-to-concrete interfaces. J Geotech Geoenviron Eng 129(11):993–1000
21. Goodman RE, Taylor RL, Brekke TL (1968) A model for the mechanics of jointed rock. J Soil Mech Found Div 94(SM 3):637–659 **(Proc. Paper 5937)**
22. Gudehus G (1996) A comprehensive constitutive equation for granular materials. Soils Found 36(1):1–12
23. Gutjahr S (2003) Optimierte Berechnung von nicht gestützten Baugrubenwänden in Sand. Ph.D. thesis no. 25, TU Dortmund
24. Herle I, Gudehus G (1999) Determination of parameters of a hypoplastic constitutive model from properties of grain assemblies. Mech Cohesive-Frict Mater 4:461–486
25. Herle I, Nübel K (1999) Hypoplastic description of interface behaviour. In: Pande G, Pietruszczak S, Schweiger H (eds) Numerical models in geomechanics—NUMOG VII. A.A.Balkema, Graz, pp 53–58
26. Hu L, Pu J (2004) Testing and modeling of soil–structure interface. J Geotech Geoenviron Eng 130(8):851–860
27. Hu L, Pu JL (2003) Application of damage model for soil–structure interface. Comput Geotech 30(2):165–183
28. Jaky J (1948) Pressure in silos. In: 2nd ICSMFE, pp 103–107
29. Kolymbas D (1977) A rate-dependent constitutive equation for soils. Mech Res Commun 4(6):367–372
30. Koval G, Chevoir F, Roux JN, Sulem J, Corfdir A (2011) Interface roughness effect on slow cyclic annular shear of granular materials. Granul Matter 13(5):525–540
31. Lashkari A (2013) Prediction of the shaft resistance of nondisplacement piles in sand. Comput Geotech 37(January 2012):904–931
32. Liu H, Song E, Ling HI (2006) Constitutive modeling of soil-structure interface through the concept of critical state soil mechanics. Mech Res Commun 33(4):515–531

33. Liu J, Zou D, Kong X (2014) A three-dimensional state-dependent model of soil-structure interface for monotonic and cyclic loadings. Comput Geotech 61:166–177
34. Martinez A, Frost JD, Hebeler GL (2015) Experimental study of shear zones formed at sand/steel interfaces in axial and torsional axisymmetric tests. Geotech Test J 38(4):1–20
35. Mascarucci Y, Miliziano S, Mandolini A (2014) A numerical approach to estimate shaft friction of bored piles in sands. Acta Geotech 9(3):547–560
36. Matsuoka H, Nakai T (1974) Stressdeformation and strength characteristics of soil under three different principal stresses. Proc Jpn Soc Civ Eng 232:59–70
37. Niemunis A, Herle I (1997) Hypoplastic model for cohesionless soils with elastic strain range. Mech Cohesive-Frict Mater 2(1997):279–299
38. Peng SY, Ng CWW, Zheng G (2013) The dilatant behaviour of sandpile interface subjected to loading and stress relief. Acta Geotech 9(3):425–437
39. Porcino D, Fioravante V, Ghionna VN, Pedroni S (2003) Interface behavior of sands from constant normal stiffness direct shear tests. Geotech Test J 26(3):1–13
40. Potyondy JG (1961) Skin friction between various soils and construction materials. Géotechnique 11:339–353
41. Shahrour I, Rezaie F (1997) An elastoplastic constitutive relation for the soil–structure interface under cyclic loading. Comput Geotech 21(1):21–39
42. Taha A, Fall M (2014) Shear behavior of sensitive marine clay-steel interfaces. Acta Geotech 9(6):969–980
43. Tejchman J, Wu W (1995) Experimental and numerical study of sandsteel interfaces. Int J Numer Anal Methods Geomech 19(March 1993):513–536
44. Uesugi M, Kishida H (1986) Frictional resistance at yield between dry sand and mild steel. Soils Found 26(4):139–149
45. Uesugi M, Kishida H, Tsubakihara Y (1988) Behavior of sand particles in sand–steel friction. Soils Found 28(1):107–118
46. Weißenfels C, Wriggers P (2015) A contact layer element for large deformations. Comput Mech 55(5):873–885
47. Weißenfels C, Wriggers P (2015) Methods to project plasticity models onto the contact surface applied to soil structure interactions. Comput Geotech 65:187–198
48. Wernick E (1978) Skin friction of cylindrical anchors in non-cohesive soils. In: Symposium on soil reinforcing and stabilising techniques in engineering practice, Sydney, Australia, October 16–19, pp 201–219
49. von Wolffersdorff PA (1996) Hypoplastic relation for granular materials with a predefined limit state surface. Mech Cohesive-Frict Mater 1(3):251–271
50. Wu W (1992) Hypoplastizität als mathematisches Modell zum mechanischen Verhalten granularer Stoffe. Ph.d thesis no. 129, Institut für Bodenmechanik und Felsmechanik der Universität Fridericiana in Karlsruhe
51. Wu W, Bauer E (1994) A simple hypoplastic constitutive model for sand. Int J Numer Anal Methods Geomech 18:833–862
52. Zaman MM, Desai CS, Drumm AM (1984) Interface model for dynamic soil–structure interaction. J Geotech Eng 110:1257–1273
53. Zeghal M, Edil TB (2002) Soil structure interaction analysis: modeling the interface. Can Geotech J 39(3):620–628